Electronic Supplementary Material (ESI) for ChemComm.

Supplementary information:

Geometry twisted intra-inter molecular cooperative interactions for enhanced photo-response in ORMOSIL based host-guest system

Moumita Chandra, Alpana Sahu, Nitul Kalita and Mohammad Qureshi*

Materials Science Laboratory, Department of Chemistry,
Indian Institute of Technology Guwahati, Guwahati-781039

E-mail: mq@iitg.ac.in

Table of contents

1. EXPERIMENTAL SECTION

Materials. All chemicals utilized in the experiments were of analytical grade. Milli-Q water was employed for solution preparation. Sodium hydroxide and tetraethylorthosilicate (TEOS) were procured from Merck, while 2-(2-hydroxyphenyl benzothiazole) and vinyltrimethoxysilane (VTMOS) were obtained from Sigma-Aldrich.

Synthesis of organically modified silica (ORMOSIL)

A solution containing tetraethylorthosilicate (TEOS) and vinyltrimethoxysilane (VTMOS) in a 1:3 molar ratio was prepared and hydrolyzed for 3 hours. To this solution, 1 M NaOH solution was introduced dropwise for base hydrolysis and further stirred for 1 hr. The obtained white-coloured thick liquid was further stirred for another 1 h and then dried in an oven at 60 ^{o}C for

12 h. The hydrolysis and condensation reaction mechanism of the precursors for the formation of ORMOSIL are explained below:

Hydrolysis-

$$Si(OCH_2CH_3)_4 \rightarrow Si(OH)_4 \quad (i)$$

$$(OCH_3)_3Si\,CH=CH_2 \rightarrow (OH)_3Si\,CH=CH_2 \quad (ii)$$

Condensation-

$$Si(OH)_4 + (OH)_3Si\,CH=CH_2 \rightarrow (OH)_3Si-O-Si(OH)_2CH=CH_2 \quad (iii)$$

Synthesis of ORMOSIL-HBT composite

For the synthesis of composite a prerequisite amount of HBT (2 mmol, 4 mmol and 6 mmol) was added in the solution of TEOS and VTMOS and stirred for 3 h. Then, 1 M NaOH solution was introduced dropwise for base hydrolysis and further stirred for 1 hr. The obtained white colour product was then transferred in a hot air oven maintained at 60 °C for 12 hours. The sample was coded as ORH2, ORH4, and ORH6.

Material Characterization

The crystal structure were assessed using a 9 kW rotating anode powder X-ray diffractometer (Rigaku Smart Lab) equipped with a Ni filter and Cu-K_α X-ray source (wavelength: 1.5406 Å). Morphology and microstructure analysis were conducted using a field emission scanning electron microscope (Zeiss Sigma 300, operating voltage: 5 kV) and a field emission transmission electron microscope (JEOL microscope JEM2100F, operating voltage: 200 kV). Surface area measurements were performed using a Quantachrome Instrument (Model Autosorb, IQ MP). The photoelectrochemical performance of the synthesized materials was evaluated using the Gamry potentiostat 1010E Interface electrochemical workstation.

Photocurrent study

The photocurrent study was carried out with a conventional three electrode configuration using 0.5 M Na_2SO_4 as an electrolyte. For the preparation of working electrode, 5 mg of as-synthesized powder catalyst was well dispersed by ultrasonication in 1 mL ethanol and ultrasonicated for 20 min. Then 5 µL nafion solution was added as a binder and sonicated for

another 20 min. Then the as-prepared slurry was drop casted on fluorine-doped tin oxide (FTO) substrates (1cm × 1cm) with similar film thickness and dried. The as-prepared FTO was used as working electrode alongside Pt wire and Ag/AgCl as counter electrode and reference electrode, respectively.

2. FESEM analysis:

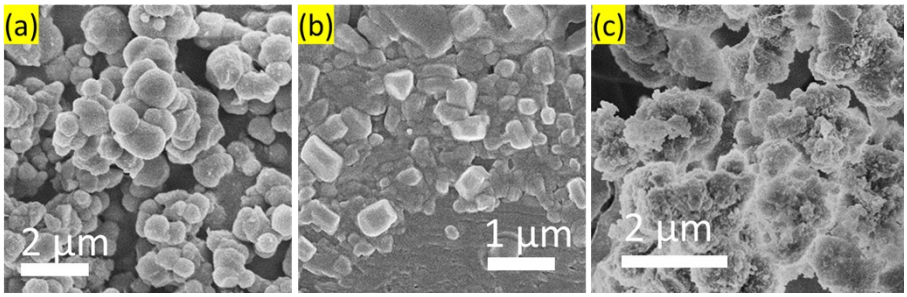

Figure S1. FESEM image of (a) pure ORMOSIL, (b) HBT and (c) ORH4.

Morphology of the as-synthesized catalyst was analysed via FESEM and the synthesis condition led to the formation of spherical ORMOSIL nanostructure as shown in Fig. S1a and HBT shows aggregated nanoparticles structure (Fig. S1b). FESEM image of the ORH4 composite displayed that the HBT nanoparticles attached to the site of ORMOSIL network (Fig. S1c).

3. EDX and XRD analysis:

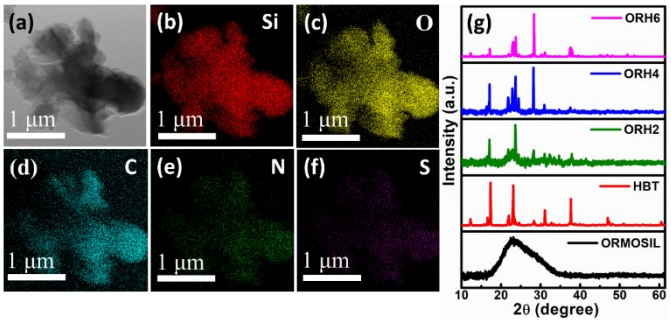

Figure S2. (a) FETEM image and (b-f) EDX elemental mapping of ORH4; (g) XRD pattern as-synthesized catalysts.

EDX elemental analysis displayed presence of all the elements in the composite ORH4 as shown in Fig. S2a-f which confirm that the HBT uniformly distributed over the ORMOSIL matrix. The structural property of the as-synthesized catalyst was studied by powder XRD, as illustrated in Fig. S2g. In its pure form, HBT displayed a distinct pattern in XRD while pure

ORMOSIL exhibits a broad peak around 2θ~23° indicating its amorphous nature. However, in the composite both materials' characteristic diffraction patterns are present. Moreover, as the proportion of HBT in the composite increases, the broad pattern of ORMOSIL diminishes, suggesting the uniform incorporation of HBT nanostructures within the ORMOSIL framework without altering its chemical nature.

4. FT-IR analysis:

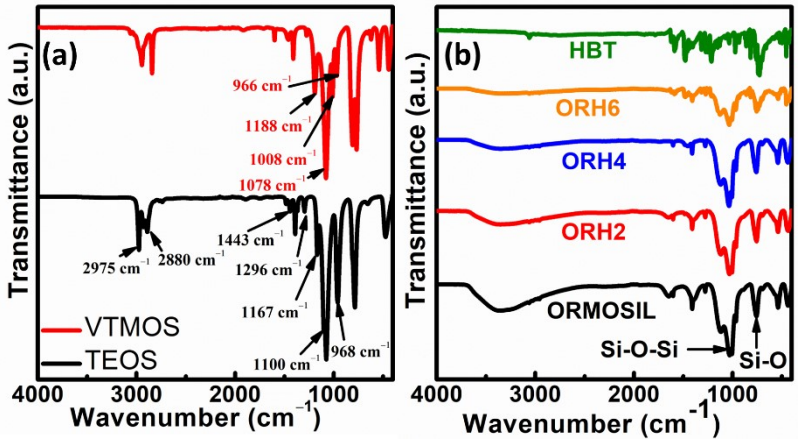

Figure S3. FT-IR spectra of (a) TEOS and VTMOS; and (b) ORMOSIL and all the materials.

FT-IR is an essential tool for effectively identifying functional groups within the material. TEOS shows typical peaks between 2975 and 2880 cm^{-1} representing C–H stretching vibration in the ester group, whereas peaks between 1443 and 1296 cm^{-1} related to asymmetric bending or wagging of C–H bonds.[1] The peaks around 1167 and 968 cm^{-1} correspond to C–H rocking. The Si atom bound to the ethoxy group (Si–OCH_2CH_3) is represented by peaks around 1100 cm^{-1}. At a wavenumber 788 cm^{-1} attributed to the oscillation of Si–C bond. In VTMOS (Figure S3a), the spectra recorded at 1078 cm^{-1} and 1188 cm^{-1} attributed to the methoxy group whereas vinyl group appear at 1008 cm^{-1} and 966 cm^{-1}.[2] In VTMOS Two bands of low intensity appear at 3062 and 2959 cm^{-1} attributed to the asymmetrical and symmetrical stretching vibration of $=CH_2$ respectively. The absorption band at 1605 cm^{-1} is attributed to the C=C vibration of the terminal olefin group whereas 1407 cm^{-1} is associated with vinyl CH_2 in-plane deformation. HBT shows absorption band at 1260, 1501, and 685 cm^{-1} are ascribed to stretching of C–O, N=C–S, and C–S respectively (Fig. S3b) and a band at 1598 cm^{-1} suggested C=N stretching.[3,4] The band observed at about 3070 cm^{-1}

assigned as an intramolecular hydrogen bond connecting hydroxyphenyl and benzothiazole moieties. Fig. S3b shows the FT-IR pattern of all the materials.

5. UV-Vis analysis:

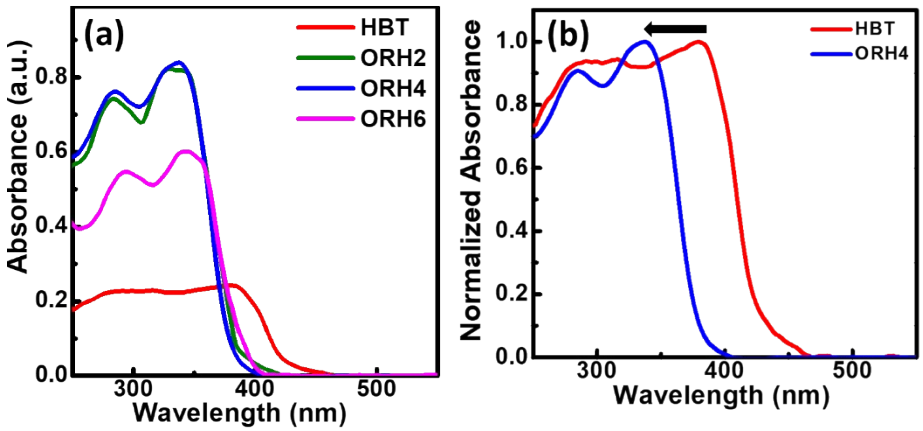

Fig. S4. (a) Pure HBT shows well-resolved UV-Vis spectra with maximum absorbance in the range of 380 nm. After the formation of composite absorbance shifted toward lower wavelength region as indicated by the arrow as shown in Fig. S4b.

6. Photocurrent study

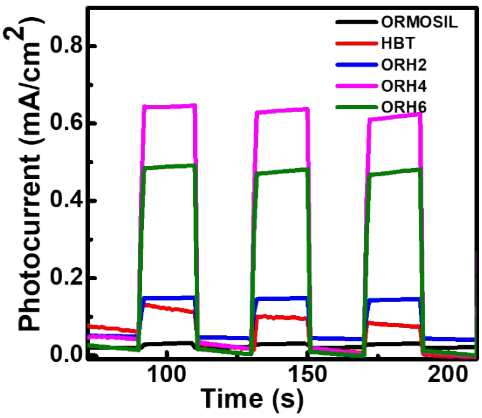

Fig. S5: Photocurrent measurement of ORMOSIL-HBT composite with varying concentrations of HBT.

The chronoamperometry analysis was carried out using the as-synthesized catalysts in a solution of 0.5 (M) Na_2SO_4 under 1 Sun illumination at 20 s chopping interval. A fast photocurrent response was observed and ORH4 gives the highest photocurrent density of 0.65 mA/cm^2 as compared to ORH2 and ORH6 as shown in Fig. S5 at a fixed potential 0.7 V (vs Ag/AgCl) which is 21 and 5 times greater than ORMOSIL and HBT

7. TRPL fitting analysis

TRPL decay was fitted with a bi-exponential decay model according to the following equation:

$$I = A_1 e^{-t/\tau_1} + A_2 e^{-t/\tau_2}$$

Here, I represent the normalized PL intensity, A_1 and A_2 represent the component percentage, and τ1 and τ1 represent the respective exciton lifetime for different carrier kinetic processes. The average lifetime is calculated using the following expression:

$$\tau_{avg} = \frac{A_1\tau_1^2 + A_2\tau_2^2}{A_1\tau_1 + A_2\tau_2}$$

Table S1. The values of fitting parameters: exciton lifetimes (τ_1, τ_2,), pre-exponential factors (A_1, A_2) and calculated values of average exciton lifetimes (τ) (ns)

Sample	τ_1 (ns)	τ_2 (ns)	A_1	A_2	Average lifetime (τ) (ns)
HBT	0.45	4.6	8.5	91.5	4.5
ORH4	1.12	3.18	22	78	2.9

The average lifetime of the composite ORH4 decreases as compared to pure HBT which indicates efficient charge separation and reduced recombination in the catalyst.

8. Mott–Schottky analysis

The Mott–Schottky plots were obtained for the as-synthesized photocatalysts using the following equation

$$\frac{1}{C^2} = \frac{2}{q\varepsilon\varepsilon_0 N_D}\left(E - E_{fb} - \frac{kT}{q}\right)$$

Here *C*, ε_0, q and N_D represent space charge capacitance, permittivity in vaccum (8.85×10^{-14} F cm^{-2}), charge of an electron, and semiconductor donor density, respectively. ε is the dielectric constant of material, *k*, *T*, *E* and E_{fb} are the Boltzmann constant, temperature (in Kelvin), applied potential, and flat band potential, respectively. Moreover, the carrier density was measured by using the following equation:

$$N_D = \frac{2}{\varepsilon\varepsilon_0 q} \times \left(\frac{dE}{dC^2}\right) = \frac{2}{\varepsilon\varepsilon_0 q} \times \left(\frac{1}{slope}\right)$$

ORH4 shows a smaller slope than pure ORMOSIL suggesting more carrier density, and better photocurrent density.

9. NMR analysis

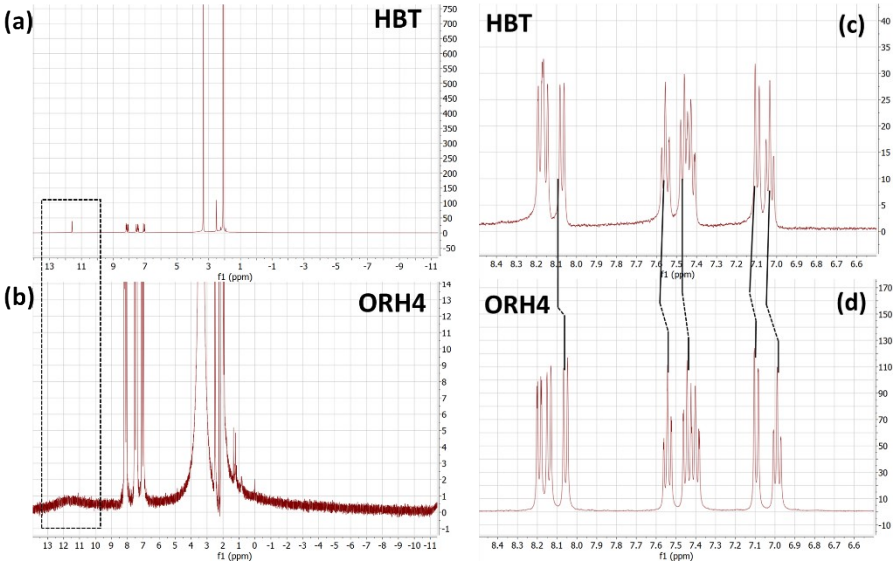

Fig S6. 1H-NMR spectra in DMSO-d6 of (a, c) HBT and (b, d) ORH4, showing the reduced peak intensity of –OH proton in the composite.

DMSO-d_6 used as a solvent for NMR study. Peaks in the range of δ= 6.5 to 8.5 ppm belong to the 7 protons attached to the aromatic ring (Ar–H) and are seen as singlet, doublet, doublet-doublet and triplet peaks (Fig. S6a). The singlet peak observed at δ= 11.55 ppm belongs to the (–OH) proton which is due to the intramolecular hydrogen bonding.[5] After the formation of the HBT-ORMOSIL matrix, a significant reduction in the singlet peak intensity as well as shifting of (–OH) proton towards the deshielded region is observed indicating the disruption of intramolecular hydrogen bonding in HBT and intermolecular interactions in the caged structure of ORMOSIL matrix with the –OH group of HBT as shown in the Fig. S6b. Additionally, a significant shift in NMR spectra of the aromatic region implies that the interaction of HBT with ORMOSIL matrix in the composite and changes in aromatic environment (Fig. S6c-d) and implies intermolecular interaction between HBT and ORMOSIL matrix.

1. A. Hadela, M. Lakić, M. Potočnik, A. Košak, A. Gutmaher and A. Lobnik, *Adsorpt. Sci. Technol.*, 2020, **38**, 168.
2. S. S. Abbas, G. J. Rees, N. L. Kelly, C. E. J. Dancer, J. V. Hanna and T. McNally, *Nanoscale*, 2018, **10**, 16231–16242.

3. M. Güçoğlu and N. Şatıroğlu, *J. Mol. Liq.*, 2022, **348**, 118388.
4. M. Jumaah, M. Khairuddean and S. J. Owaid, *J. Fluoresc.*, 2022, **32**, 937–948.
5. S. Sahana, G. Mishra, S. Sivakumar, and P. K. Bharadwaj, *Dalton Trans.*, 2015, **44**, 20139-20146.